Design and Performance of Propellers and Pumpjets for Underwater Propulsion

B. W. McCormick* and J. J. Eisenhuth†
Pennsylvania State University, University Park, Pa.

This paper treats the design and presently attainable performance of propellers and pumpjets as they are applied to the propulsion of torpedoes and submarines. Consideration is given to both cavitation and efficiency requirements. Primary emphasis is given to the consideration of pumpjets because of the present lack of literature on methods of pumpjet design.

Nomenclature

A = propeller disk area
A_R = rotor disk area
B = number of blades
c = chord length
c_a = axial projection of chord length
c_d = section drag coefficient
C_D = body drag coefficient
c_l = section lift coefficient
$c_{l\infty}$ = section lift coefficient for infinite blade spacing
C_P = power coefficient
c_p = pressure coefficient
c_{pR} = pressure coefficient immediately upstream of rotor
c_{pu} = pressure coefficient for suction surface of blade
C_Q = torque coefficient
C_T = thrust coefficient $= T/\frac{1}{2}\rho V_0^2 \pi R_T^2$
C_{T_R} = thrust coefficient of rotor
D = drag, diameter
$D_{1/4}$ = shroud diameter at $\frac{1}{4}$ chord point
$D_{3/4}$ = shroud diameter at $\frac{3}{4}$ chord point
J = advance ratio
L = lift per unit span
m = mass flow rate
n = rotational speed, rps; normal distance between streamlines
Δn = distance between camber line and mean streamline measured normal to the chord line
Δn_1 = Δn for $c_l = 1.0$
P = power
p = pressure
p_0 = freestream static pressure
p_R = static pressure immediately upstream of rotor
p_u = static pressure at suction surface of blade
p_v = vapor pressure of water
r = radius
R = rotor radius
R_I = outer radius of pumpjet "inner region"
R_p = propeller radius
R_T = body radius
R_1 = shroud radius at the inlet
$R_{1/4}$ = shroud radius at $\frac{1}{4}$ chord point
s = reciprocal of section solidity
T = thrust
T_R = thrust of rotor
T_S = thrust of shroud
t = section thickness, tangential projection of section thickness
u = tangential component of induced velocity
$\mathbf{U}$ = velocity of runner
V = axial velocity, otherwise as defined in text
$\mathbf{V}$ = absolute fluid velocity
$\bar{V}$ = equivalent constant velocity
v = velocity induced tangentially to mean camber line
$V(r)$ = axial velocity in boundary layer of body
V_e = resultant velocity at propeller blade section
v_i = velocity induced by shroud at $\frac{3}{4}$ chord point
v_{iR} = radially inward component of velocity induced by rotor
V_m = mean axial velocity in boundary layer of body, meridional velocity
V_0 = freestream velocity
V_R = velocity at rotor
V_3 = velocity far downstream of propulsor
V_∞ = mean or reference velocity for cascade
V_θ = tangential component of velocity
w' = velocity of advance of vortex sheet
$\mathbf{W}$ = velocity relative to runner
$w(x)$ = axially induced velocity of unshrouded rotor
w_a = axially induced velocity at propeller blade
w_t = tangential induced velocity at propeller blade
W_θ = tangential component of relative velocity to runner
x = relative radius ($= r/R_p$), axial distance, relative axial distance (= axial distance/chord)
y_c = circumferential coordinate of mean camber line
y_m = circumferential coordinate of mean streamline
z = maximum camber dimension
α_h = angle that undisturbed streamline at R_1 makes with respect to body axis
β = stagger angle of cascade
Γ = circulation
γ = angle that shroud chord line makes with body axis
$\boldsymbol{\zeta}$ = vorticity vector
η = propeller "efficiency"
η_i = ideal efficiency
η_T = true propeller efficiency
κ = Goldstein's factor
λ_m = $\omega r/V_m$
μ_h = $\pi x_h/J$
μ_0 = π/J
ρ = mass density
σ = cavitation index, section solidity
σ_B = critical cavitation index of blade tip section
σ_c = critical cavitation index
σ_0 = freestream cavitation index
σ_R = cavitation index before rotor
σ_S = cavitation index before stator
σ_t = critical cavitation index due to thickness
τ = thrust deduction fraction
φ = angle of propeller section resultant velocity
ω = rotational velocity

Presented at the ARS 17th Annual Meeting and Space Flight Exposition, Los Angeles, Calif., November 13–18, 1962; revision received July 25, 1963. The authors would like to acknowledge the efforts of many members of the staff of the Garfield Thomas Water Tunnel in the conduct of the experimental and analytical developments presented in this paper. In particular, the authors wish to note the contributions of George F. Wislicenus to the design of the pumpjet and to the theory of rotational flow through fixed and rotating vane systems. Finally, they wish to thank the U. S. Naval Bureau of Weapons for their support of this program.

* Professor of Aeronautical Engineering. Member AIAA.
† Research Associate, Ordnance Research Laboratory, presently with the Curtiss-Wright Corporation. Associate Member AIAA.

Introduction

THE design of a submarine or torpedo propulsor is influenced to a large extent by the shape of the hull on which

it is to operate. The propulsor is submerged completely within the boundary layer of the hull and must be designed for this radially nonuniform inflow. A wake-operating propulsor designed for one body shape cannot be expected to produce comparable performance on another body. Open-water tests of wake-operating propulsors are meaningless unless a radially varying inflow that simulates the boundary layer of the body is produced by artificial means. The first step in the design of a wake-operating propeller or pumpjet is to determine the velocity profile in which it is to operate.

For a given body, the thrust that must be produced by the propelling device exceeds the bare body drag and is given by

$$T = D(1 + \tau) \tag{1}$$

The factor τ is referred to as the thrust deduction fraction. Methods of estimating τ for a propeller-body combination can be found in the literature.[1,2] Normally, for torpedoes, τ will be approximately 0.10 to 0.15.

It is convenient to deal with the thrust in terms of the coefficient defined as

$$C_T = T/\tfrac{1}{2}\rho V_0^2 \pi R_T^2 \tag{2}$$

where V_0 equals the velocity of the body, and R_T equals the body radius. The use of the body radius rather than the propeller radius serves to emphasize the fact that the propeller and body cannot be separated. A body drag coefficient is defined in the same way as Eq. (2), and a power coefficient can be defined by changing V_0 to the third power in the denominator.

Propellers

This presentation will be limited to general remarks on the design of propellers. Detailed methods of designing both single and counterrotating propellers can be found in the literature.[1] The methods that are used in Ref. 1 are based upon the vortex theory of propellers as developed by Goldstein,[3] with suitable corrections to account for finite hub size and for the differences between a lifting line and the finite blade it replaces.

An extension to Goldstein's analysis was made to the case where the hub radius is appreciable relative to the propeller radius.[5] The typical effect of the addition of a hub to Goldstein's solution is shown in Fig. 1. Corrections to be applied to Goldstein's factors for the hub effect are given in Refs. 1 and 14. It can be seen in Fig. 2 that the circulation is increased toward the hub and has a zero gradient in the radial direction at the hub surface.

A blade with a finite chord, when replaced by a lifting line, will not have sufficient camber to produce the lift that is needed. Various corrections to the camber have been developed. An approximate correction, which can be applied graphically during the drafting layout process, is presented in Ref. 1. This correction assumes that the tangential component of induced velocity varies linearly from a value of zero at the leading edge of each section to its full value of $2w_t$ at the trailing edge. If the blades are closely spaced, it may also be necessary to take into account the thickness effect or constriction of the flow in the axial direction.

A theory is developed in Ref. 4 for the optimum distribution of bound circulation for a single, wake-adapted propeller. This theory ignores, however, any effects due to the maintaining of a finite amount of bound circulation at the surface of the hub. Propellers designed to have this optimum distribution of bound circulation were found to produce a strong hub vortex. The low pressure in the core of this vortex, acting over the after-face of the hub, detracted appreciably from the thrust produced by the propeller blades. Propellers designed with the circulation arbitrarily reduced toward the hub have given better efficiency than the "optimum" propellers because of the elimination of the hub vortex.

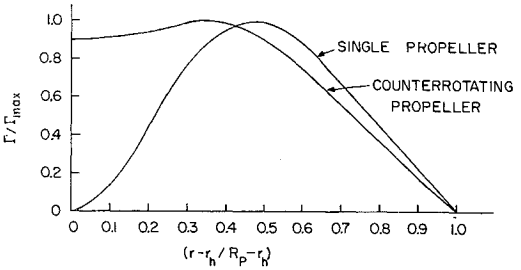

Fig. 1 Typical bound circulation distributions.

Cavitation, as well as thrust and power, must be considered in designing a marine propeller. Cavitation is defined as the formation of vapor-filled cavities in a flowing liquid due to local reductions in pressure. These cavities, which form in a region of low pressure where the pressure has been reduced to approximately the vapor pressure of the fluid, are swept into regions of higher pressure where they collapse. This collapse causes either noise, mechanical damage, or a loss in efficiency, depending upon the severity of the cavitation.

The intensity of cavitation is related to the cavitation index defined by

$$\sigma = (p_0 - p_v)/\tfrac{1}{2}\rho V_0^2 \tag{3}$$

Except for scale effects, there is a particular value of the foregoing coefficient known as the critical cavitation index σ_c below which cavitation will occur on a given body shape. If the operating index σ is greater than σ_c, cavitation will not be present on the body; but, if σ is less than σ_c, the vapor pressure will have been reached at some point on the body, and cavitation will occur.

Because of the high relative velocities experienced by propeller blade sections, the problem of designing a propeller with a low critical index requires considerable attention to detail. The more important factors in a design which affect cavitation performance are: 1) alignment of the blade sections with the relative flow; 2) choice of blade section shapes; 3) choice of design advance ratio ($J = V_0/nD$); 4) solidity; and 5) radial distribution of bound circulation.

The sections that are recommended are the NASA airfoils with uniform chordwise pressure distribution such as the 16 or 65 series. The advance ratio should be as high as possible when designing for good cavitation performance. Higher advance ratios for given forward speeds mean lower rotational speeds and consequently lower relative speeds. Advance ratios of 2.5 to 3.0 are common for good cavitation performance. The choice of solidity is tied in closely with the advance ratio. For a given thrust and level of cavitation performance, larger chords are needed with higher design advance ratios to maintain a satisfactory ratio of thrust to projected blade area in a plane normal to the body axis.

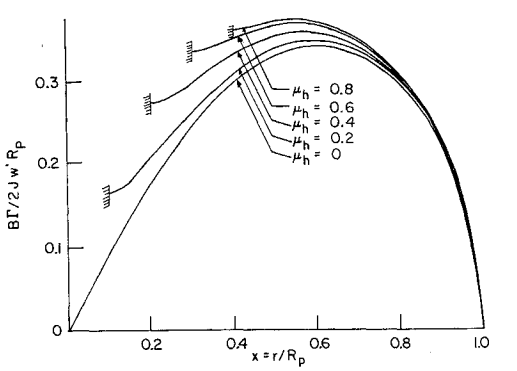

Fig. 2 Effect of finite hub on bound circulation of an optimum propeller.

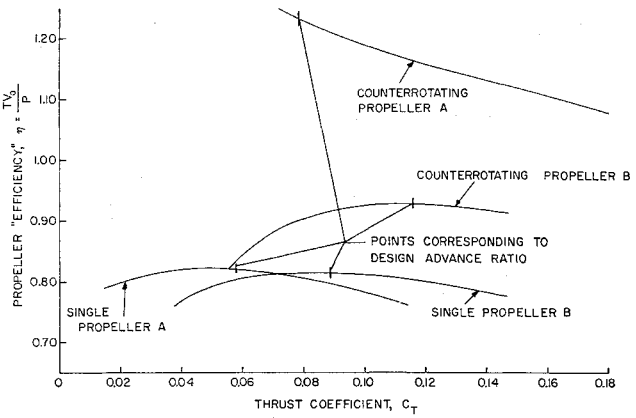

Fig. 3 Performance of representative wake-adapted propellers.

The radial distribution of bound circulation, previously mentioned with respect to efficiency, must also be reduced toward the hub to eliminate the cavitating hub vortex as a problem. Generally, for a single propeller, the type of distribution shown in Fig. 1 is used. The gradual reduction of the circulation to zero at the tip is again dictated by both cavitation[6] and efficiency considerations. If a counterrotating set of propellers or a system of single propeller and countervanes is considered, the rotational components of induced velocity are canceled in the mean so that there is no restriction as to heavy inboard loading. A typical distribution for a counterrotating propeller is shown in Fig. 1.

Attainable levels of efficiency for wake-operating propellers are presented in Fig. 3. A word of explanation should be made with regard to efficiency as used here. In Fig. 3 propeller "efficiency" is defined as

$$\eta = TV_0/P = C_T/C_P \tag{4}$$

By this definition, it is possible for η to exceed unity. The explanation of this lies in the fact that the propeller, in producing its thrust, is exposed to an inflow velocity that in the mean is less than V_0. The true useful power should be the thrust times some mean velocity v_m. As defined in Eq. (4), η could be written as

$$\eta = (TV_m/P)\cdot(V_0/V_m) = \eta_T(V_0/V_m) \tag{5}$$

where η_T is defined as true propeller efficiency. The ratio

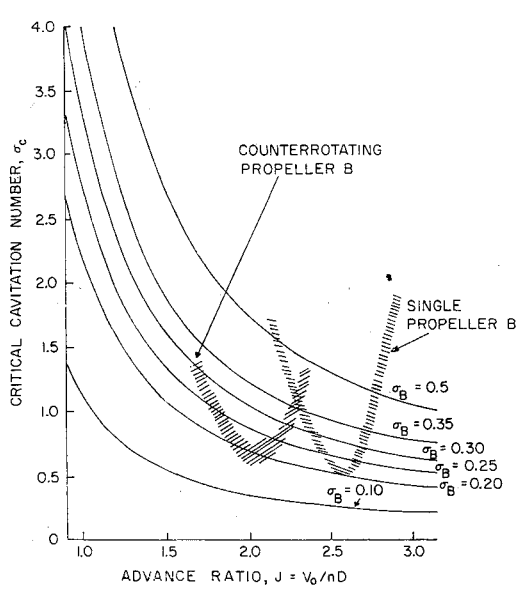

Fig. 4 Cavitation characteristics of propulsors as a function of advance ratio.

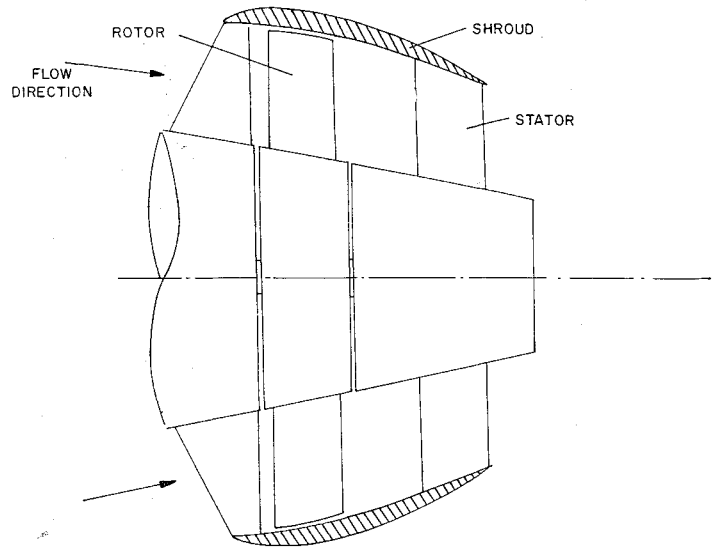

Fig. 5 Schematic of pumpjet.

V_0/V_m is always greater than one and, if large enough, permits η to be greater than one.

In Fig. 3, the two propellers A were designed primarily with efficiency as the criterion and the propellers B with good cavitation performance as the goal. The single propeller A was designed using heavy loading inboard as given in Ref. 4. The single propeller B was designed with a distribution similar to the one shown in Fig. 1. The maximum efficiency of these two propellers is not too much different, even though the B propeller had a greater solidity and consequent higher profile losses and was not designed with an "optimum" circulation distribution. This helps to verify the previous statements about loading distributions and the effect of a strong hub vortex.

The performance of counterrotating propellers shows the gains to be realized by loading heavily inboard and eliminating rotational losses from the system. Counterrotating propeller A is an example of a propeller that can have an "efficiency" greater than unity.

The cavitation performance that might be expected of propellers is shown in Fig. 4. This family of curves, taken from Ref. 7, shows the critical cavitation numbers that might be expected for different advance ratios. The values associated with the curves are values of the critical cavitation numbers of the blade tip sections based on the relative tip speed; σ_B is related to σ_c by

$$\sigma_c = \sigma_B[1 + (\omega R_P/V_0)^2] \tag{6}$$

Values of σ_B between 0.2 and 0.3 are reasonable, and so it can be expected that a propeller designed for good cavitation performance would have its critical value fall between these two curves. Figure 4 shows graphically the importance of using higher design advance ratios.

Pumpjets

The design of pumpjets is currently receiving considerable attention in the technical literature. Design methods for such propulsors are far from being firmly established. Morgan's approach[8] is representative of one general type of analysis to be found in the literature. Here the shroud and propeller are replaced by an equivalent system of ring sources and sinks, ring vortices, and vortex filaments. The ultimate solution is performed numerically by means of a digital computer. As yet, a method has not been developed for directly obtaining an optimum pumpjet design. Instead, one must perform a series of designs in order to select the one that satisfies his requirements.

The type of pumpjet which will be considered is shown schematically in Fig. 5. It consists of a rotating blade row, or rotor, followed by a stationary blade row, or stator. The rotor and stator are enclosed by a shroud. The whole assembly is mounted on the aft end of an axisymmetric body and operates in the boundary layer of the body. Within limits, it is possible to control the velocity and static pressure at the rotor by suitable shaping of the shroud.

Insight into the operation of a pumpjet can be gained by the application of fundamental momentum relationships. Consider Fig. 6a. Here the flow through a pumpjet is superimposed over the flow through an open propeller. Both the propeller and pumpjet are designed for the same mass flow rate and velocity in the ultimate wake, V_3. The propeller has a disk area of A, whereas the disk area of the pumpjet rotor is $A + \Delta A$. It can be shown from momentum considerations that the ratio of rotor thrust to net thrust of the unit is given by

$$T_R/T = 1/\eta_i(1 - c_{p_R})^{1/2} \tag{7}$$

where η_i is the ideal propeller efficiency obtained from the simple axial momentum theory, and C_{pR} is given by

$$c_{p_R} = 1 - (V_R/V_0)^2 \tag{8}$$

where V_R is the velocity at the rotor.

Equation (7) shows that, for a given net thrust, the required rotor thrust increases as the static pressure at the rotor is increased. Hence, although one might feel that diffusing the flow up to the rotor will improve its cavitation performance by increasing the local static pressure, this is not necessarily the case, since the required thrust of the rotor will also increase.

As a matter of further interest with regard to Fig. 6, the discontinuity in pressure across the disks is given by

$$\Delta p = \tfrac{1}{2}\rho(V_3^2 - V_0^2) \tag{9}$$

and the net thrust of both propulsors is the same and can be written as

$$T = m(V_3 - V_0) \tag{10}$$

where m is the mass flow rate.

Shroud Design

The shroud controls the velocity and pressure at the rotor and permits a finite loading at the tips of the blades.

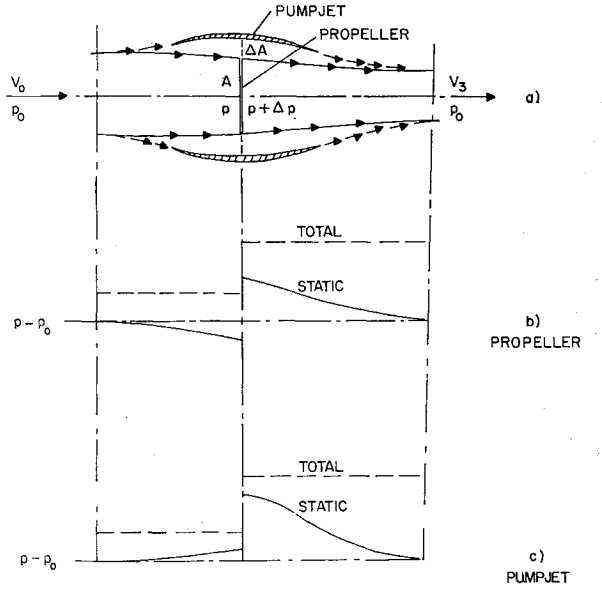

Fig. 6 Comparison of flow-through pumpjet with propeller.

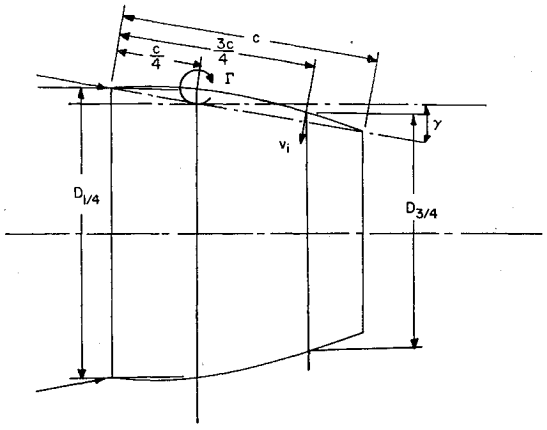

Fig. 7 Approximation to the action of a ring airfoil.

The flow, as it approaches the shroud, is either accelerated or decelerated, depending upon the application of the propulsor. In the case of a low-speed, high-static-thrust application the flow is accelerated, and one obtains the configuration of the so-called Kort nozzle. For high-speed application, the optimum geometry is usually one that diffuses the flow slightly.

Provided that the configuration is not too extreme, it is possible to estimate the negative thrust produced by the shroud relatively easily by the application of a simple artifice. This is done by replacing the shroud by a ring vortex located at its $\frac{1}{4}$ chord line and satisfying boundary conditions at the $\frac{3}{4}$ chord line. This approximation, sometimes referred to in the literature as Weissinger's approximation, is known to work well for ordinary wings and even for airfoils in cascade.

A ring airfoil is shown in Fig. 7. The convergence angle of the chord line is assumed to be small so that the axial distance between the $\frac{1}{4}$ and $\frac{3}{4}$ chord points is approximately $c/2$. Tabulated functions are given in Ref. 9 relating Γ, v_i, and the geometry of the ring. According to the reference, the velocity induced at the $\frac{3}{4}$ chord point can be expressed as

$$v_i = \frac{\Gamma}{\pi D_{1/4}} \cdot f\left[\frac{c}{D_{1/4}}, \frac{D_{3/4}}{D_{1/4}}\right] \tag{11}$$

The function $f[c/D_{1/4}, D_{3/4}/D_{1/4}]$ is taken directly from Ref. 9 and is presented in Fig. 8. The circulation must be such

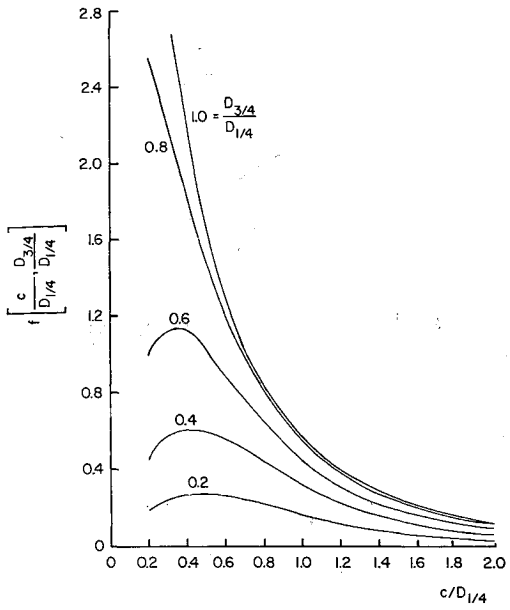

Fig. 8 Velocity induced by vortex ring.

as to induce a V_i that, when added to the freestream velocity and the velocity induced by the rotor, will produce a resultant velocity tangent to the mean camber line of the shroud at the $\frac{3}{4}$ chord line.

Once Γ is determined, the negative thrust T_S developed by the shroud can be calculated by the Kutta-Joukowski law. In calculating this thrust, consider a diffusing shroud ring on a tapered afterbody but without a rotor. In this case, a circulation is developed around a shroud section, and the local velocity without the shroud has a radial component inward. Thus, from the Kutta-Joukowski law, one might calculate a negative thrust on the shroud. However, from D'Alembert's paradox, the net axial force on the shroud body combination must be zero. Thus, any axial force on the shroud produced as a result of the product of Γ and the radial velocity induced by the body is canceled by an image system within the body. Hence, the negative thrust on the shroud in the presence of the rotor is calculated from

$$T_S = 2\pi r_{1/4}\rho\Gamma v_{iR} \tag{12}$$

From consideration of the variation of axial velocity through a propeller and of continuity it can be shown that the radial velocity induced inward by the rotor will be approximately

$$v_{iR} = \frac{V_0}{2}\left[\frac{(1 - C_{TR})^{1/2} - 1}{(1 + C_{TR})^{1/2} + 1}\right] \tag{13}$$

where C_{TR} is the rotor thrust coefficient defined in the same manner as C_T in Eq. (2).

The use of the foregoing developments is complicated by the fact that the pumpjet on a torpedo or submarine is submerged in the boundary layer developed at the body. To correct for this, an equivalent uniform velocity is used, defined by

$$\bar{V} = V_0\left[\frac{1}{A}\int_A \left(\frac{V}{V_0}\right)^2 dA\right]^{1/2} \tag{14}$$

The design of the shroud is further complicated by the fact that it is wrapped around a conical-shaped afterbody. Because it is tapered, the undisturbed stream surfaces are generally conical. Secondly, it constricts the flow through the shroud effectively increasing c/D, the chord-diameter ratio. An indication of the percentage decrease in the induced velocity in Eq. (11) can be obtained from Fig. 9, taken from Ref. 10. The ratio of lift coefficient with a centerbody to the lift coefficient without a centerbody should be identical to the ratio of the corresponding induced velocities. Hence, any v_i value calculated by Eq. (11) should be decreased by the ratio of lift coefficients obtained from Fig. 9.

The tapering of the hub is accounted for by locating the chord line of the shroud with reference to the direction of the undisturbed flow. This direction can be determined if one assumes frictional effects and static pressure variation to be negligible over the axial distance of the shroud. It then is a matter of satisfying continuity.

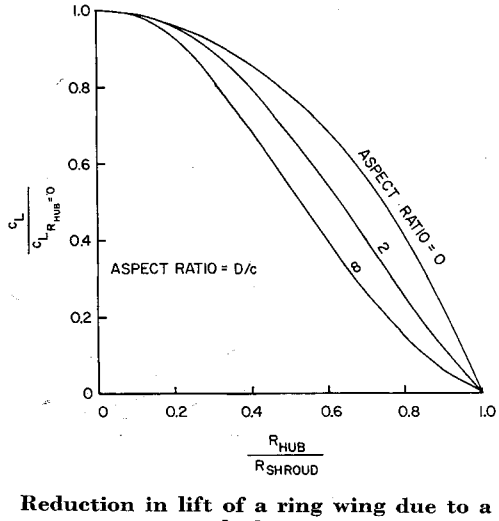

Fig. 9 Reduction in lift of a ring wing due to a center body.

To avoid negative pressure peaks at the nose, one should align the chord line of the shroud with the resultant velocity due to the body and rotor. The circulation is then obtained from camber alone. The shroud section lift coefficient should be checked. This can be calculated from

$$c_l = 2\Gamma/cV \tag{15}$$

where V equals the undiffused velocity at R. For a circular arc profile, the critical cavitation index is given approximately by

$$\sigma_c = 3(t/c) + (2c_l/\pi) \tag{16}$$

where t/c is the thickness ratio. If σ_c exceeds the operating cavitation index, then c_l will have to be decreased by either increasing c or decreasing the amount of diffusion.

In completing this part of the analysis, one should consider the possibility of stall over the outside of the shroud. The c_l of a shroud section can be used for such an estimate.

Rotor and Stator Design

From previous considerations, the velocity and pressure before the rotor and the required pressure increase across the rotor can be determined. The problem is now that of designing a rotor to produce the desired Δp without cavitating.

Euler's equation for turbomachinery takes the following form for axial-flow pumps:

$$\Delta p = \rho\omega r\Delta u \tag{17}$$

The velocity diagrams before and after a rotor are illustrated in Fig. 10. It is advisable to design for a Δu that does not exceed the linear velocity ωr. Near the root of the blade, this may not be possible to do while still maintaining a constant Δp. Hence, in an inner region one may have to limit Δu to a value of ωr. If this is the case, Δp over the rest of the rotor will have to be increased slightly in order to give an integrated value of Δp over the rotor disk area which equals the desired rotor thrust. Henceforth, the outer region will refer to the region of flow where Δp is constant, whereas the inner region will refer to the region where $\Delta u = \omega r$, so that

$$\Delta p = \rho(\omega r)^2 \tag{18}$$

In Ref. 11 kinematic conditions are developed for axially symmetric frictionless flow through fixed or rotating vanes. For most applications, the pertinent equations reduce to the following for fixed and rotating vanes, respectively:

$$\left[V_\theta\left(\frac{\partial V_\theta}{\partial r} + \frac{V_\theta}{r}\right) + V_m\left(\frac{\partial V_m}{\partial r}\right)\right]\frac{1}{\rho r V_m} = \text{constant along a streamline} \tag{19}$$

$$\left[(V_\theta - \omega r)\left(\frac{\partial V_\theta}{\partial r} + \frac{V_\theta}{r}\right) + V_m\left(\frac{\partial V_m}{\partial r}\right)\right]\frac{1}{\rho r V_m} = \text{constant along a streamline} \tag{20}$$

Before the rotor, $V_\theta = 0$, so that, for both the inner and outer regions,

$$(1/\rho r)(\partial V_m/\partial r) = \text{const} \tag{21}$$

After the rotor in the outer region, the tangential velocity V_θ is given by $V_\theta = \Delta p/\rho\omega r$, so that

$$(\partial V_\theta/\partial r) + (V_\theta/r) = 0 \tag{22}$$

Hence, in this region Eq. (21) also applies.

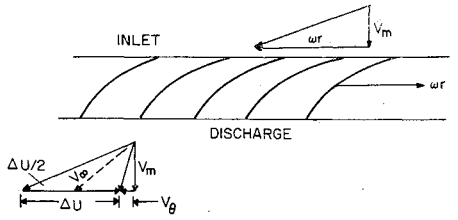

Fig. 10 Velocity diagram before and after rotor.

Along the trailing edge of the rotor in the inner region, $V_\theta = \omega r$. Hence, in this plane the velocity is related to the velocity before the rotor by Eq. (21). A practical method of applying Eq. (21) is to assume a value of V_m at some convenient radius, determine a slope of the V_m curve from Eq. (21), and then draw a tangent line to the curve at that point. The slopes at a series of radii can then be calculated and the rest of the V_m vs r curve constructed to match these slopes. A check on the original choice of a V_m value must come from continuity considerations. In other words,

$$\int_{r_h}^{R} rV_m dr = \text{const} \tag{23}$$

must be satisfied.

The tangential component V behind the rotor in the outer region can be determined by integrating Eq. (22) which leads to

$$V_\theta r = \text{constant along a streamline} \tag{24}$$

In the inner region it is assumed that the vorticity is constant on any transverse plane as it is immediately behind the rotor. It then follows from Kelvin's law of conservation of circulation that, at any transverse plane within the inner region,

$$V_\theta = \omega r \tag{25}$$

where ω is calculated from

$$\omega R_I^2 = \text{const} = \omega R_I^2 \text{ behind rotor} \tag{26}$$

where R_I is the outer radius of the inner region.

The shapes of the rotor and stator sections can be selected either by the use of available cascade data or by applying methods of designing arbitrary section shapes. Generally speaking, in order to avoid cavitation the rotor sections should be most heavily loaded toward the trailing edge where the static pressure is highest. The loading over the stator blades should be as uniform as possible.

In Ref. 13 a method is developed, referred to as "the mean-streamline method," for calculating the shape of a blade section to give a desired pressure distribution. In this method the amount of turning to be produced by each section is related to the pressure difference required by that section. With this information, a "mean-streamline" and a section camber line that departs from it can be determined.

The design of the stator proceeds in a manner similar to the rotor. However, instead of satisfying a total thrust criterion, the stator is designed to cancel the angular momentum produced by the rotor. Hence, the sections are designed so that V_θ is zero leaving the stator.

As in the case of the shroud design, the question of stall on the rotor and stator blades should not be ignored. The so-called "diffusion" limits of flow through a cascade are discussed in Refs. 12 and 13. In general, one should try to eliminate large c_l values in order to avoid separation. However, the problem in pumps is more complicated by the fact that there is a rise in static pressure across the blade row. Because separation is to a large extent determined by the pressure gradients along the fluid boundaries, this pressure rise has a decided influence on the stall characteristics. The "inner region" of the blades is particularly critical in this respect.

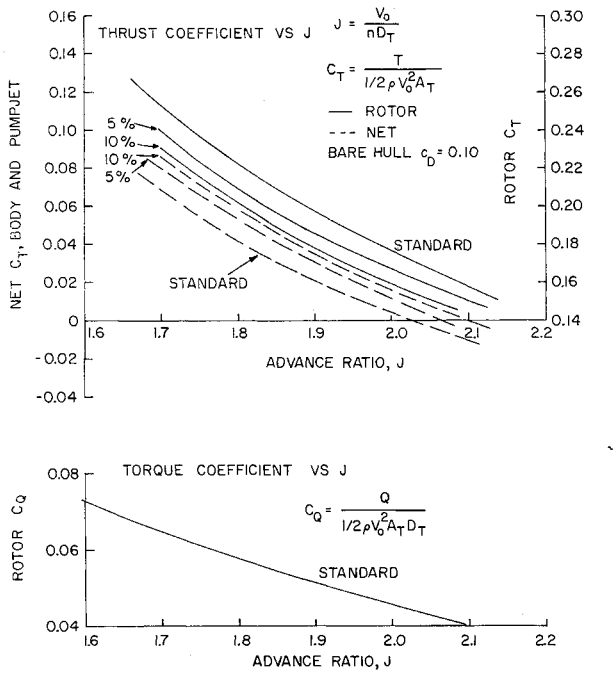

Fig. 11 Thrust and torque coefficients vs *J*.

Experimental Results

As an example, a pumpjet designed and tested at the Garfield Thomas Water Tunnel will be discussed. The rotor and stator blade sections were designed according to the "mean streamline" method so that it is difficult to present their geometry short of presenting actual drawings of each section. In general, the sections were aft loaded. Through the stator, the meridional component of velocity was increased so that the resultant velocity along the mean streamline could be kept nearly constant. This avoids having to decelerate the flow through the stator only to have it accelerate again in the jet.

At the time of its design, the drag coefficient of the body was uncertain, and the estimate that was made was too high. In addition, the considerations developed here on the design of the shroud were not available at the time of its design. Instead, the shroud was designed on the basis of approximate one-dimensional flow relationships tempered with some "art." Hence, it is somewhat superfluous to compare its originally predicted performance with the experimental results. The original design advance ratio was 1.725. At this value, a C_T of 0.216 was predicted for the unit. From Fig. 11, which presents measured thrust (obtained from axial force measurements of the body with pumpjet operating) and torque coefficients vs the advance ratio, the net C_T at a J of 1.725 is seen to be 0.061. This, added to the bare hull C_D increased 15% for thrust deduction, gives a total C_T from the pumpjet of 0.176. The difference between this and 0.216 is probably the result of negative thrust on the shroud. In spite of or maybe because of the art, the predicted net thrust coefficient does not differ too much from that which was measured. In Fig. 11, the curves labeled 5% and 10% refer to cases where the exit area of the shroud was increased by those percentages.

In a way, it was fortuitous that the unit was designed for a higher C_T than was required. This statement refers to the cavitation inception data presented in Fig. 12. When first tested at the design advance ratio, the critical cavitation indices were about 1.6 and 1.9 for rotor and stator, respectively. These were appreciably higher than the predicted values of approximately 0.7. Observations showed the blades to be suffering prematurely from suction surface cavitation on the very leading edges. Using the rate of de-

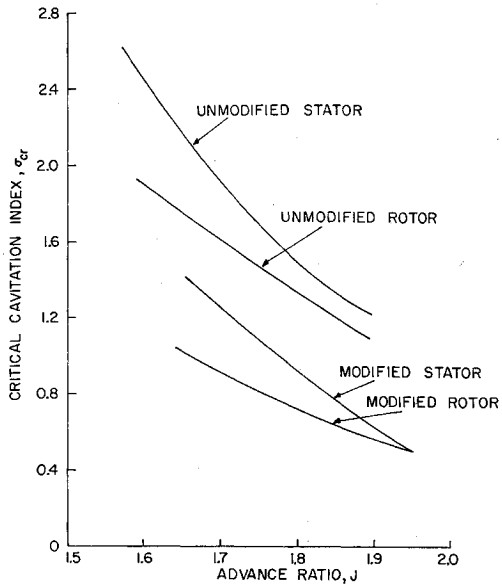

Fig. 12 Cavitation performance of pumpjet.

crease of σ_c with J as a guide, the leading edges of the blades were modified slightly to increase the slope of the mean camber line 5° in the vicinity of the leading edges. This modification, which was truly a minor alteration, produced a significant decrease in at the design J. This improvement, coupled with the fact that the J for self-propulsion ultimately proved to be 2.025, resulted in a cavitation performance that met or exceeded predictions.

Up to this point nothing has been said with regard to actual overall efficiency. One can, of course, estimate the profile drag losses of the rotor and stator and the frictional losses on the shroud which, when added to the power to produce Δp, would give the total power required. One can also consider the rotor and stator to be simply an axial flow pump and draw on the wealth of data available on axial flow pumps in order to estimate a pump efficiency. The product of the pump efficiency and the ideal or jet efficiency will then be the overall efficiency of the unit. From the torque coefficient given in Fig. 11, the propulsive efficiency of the pumpjet at self-propulsion conditions can be calculated to be

$$\eta = C_T J/2\pi C_Q = 0.833$$

As discussed in the section on propellers, this is not a true efficiency in the case of a wake-operating propulsor. As a matter of comparison, this same "efficiency" is approximately 9% higher for a single propeller behind a set of prerotation vanes designed for the same body. However, the diameter of the propeller was larger than that for the pumpjet. It would appear that, for equal disk loadings, the efficiency of the pumpjet compares favorably with the single propeller. It is true that, for the sake of mechanical complexity, the efficiency of the counterrotating propeller is better than either the single propeller or pumpjet, possibly by as much as 20% or 30%.

By performing a series of iterative calculations, the data of Fig. 11 were used to check the validity of the theory developed earlier for the diffusion afforded by the shroud. Only the standard shroud case was analyzed. In the procedure, the measured values of C_{T_R} were used to predict the diffusion and, hence, net C_T of the entire pumpjet. When this was done, it was found that the predicted increase in the net C_T as the advance ratio decreases below 2.025 is for all intents and purposes identical to the experimental results of Fig. 11. It is interesting to note that as C_{T_R} increases the magnitude of the negative C_T of the shroud increases although c_{p_R} decreases.

Conclusions

1) The efficiency and cavitation performance of a pumpjet compares favorably with a propeller.

2) Critical cavitation indices of the order of 0.5 have been attained with both pumpjets and propellers.

3) In general, the predicted performance, from the point of view of both efficiency and cavitation, agrees satisfactorily with experiment.

References

[1] McCormick, B. W., Eisenhuth, J. J., and Lynn, J. E., "A study of torpedo propellers—Part I," Ordnance Research Lab., Pennsylvania State Univ., Rept. NOrd 16597-5 (March 1956).

[2] Korvin-Kroukovsky, B. V., "Stern propeller interaction with a streamline body of revolution," Experimental Towing Tank (Davidson Lab.), Stevens Inst. Technology, Rept. 544 (September 1954).

[3] Goldstein, S., "On the vortex theory of screw propellers," Proc. Roy. Soc. (London) **A123**, 440 (1929).

[4] Lane, F., "Optimum single propellers in radially varying, incompressible inflow," J. Appl. Mech. **19**, (1952).

[5] McCormick, B. W., "The effects of a finite hub on the optimum propeller," J. Aeronaut. Sci. **22**, 645–650 (1955).

[6] McCormick, B. W., "On cavitation produced by a vortex trailing from a lifting surface," Am. Soc. Mech. Engrs. Paper 61-WA-100 (November 1961).

[7] Wislicenus, G. F., "Hydrodynamics and propulsion of submerged bodies," ARS-Preprint 1186-60 (May 1960).

[8] Morgan, W. B., "Theory of the annular airfoil and ducted propeller," 4th Symposium on Naval Hydrodynamics, Office of Naval Research, Washington, D. C. (August 1962).

[9] Kuchemann, D. and Weber, J., *Aerodynamics of Propulsion* (McGraw-Hill Book Co. Inc., New York, 1953), p. 309.

[10] Weissinger, J., "Remarks on ring airfoil theory," Armed Services Tech. Info. Agency AD 154127 (January 1958).

[11] Smith, L. H., Traugott, S. C., and Wislicenus, G. F., "A practical solution of a three-dimensional flow problem of axial-flow turbomachinery," Trans. Am. Soc. Mech. Engrs. **75**, 789–803 (July 1953).

[12] Wislicenus, G. F., *Fluid Mechanics of Turbo-Machinery* (McGraw-Hill Book Co. Inc., New York, 1947), Chap. 12.

[13] Wislicenus, G. F., "Theory and design of turbomachinery," Summer Seminar Notes, Pennsylvania State Univ. (June 22–July 3, 1958).

[14] Mercier, J. A., "Optimum propellers with finite hubs," Hydronautics Inc. TR 127-1 (June 1962).